Heliyon 10 (2024) e34023

Contents lists available at ScienceDirect

Heliyon

journal homepage: www.cell.com/heliyon

Research article

Fabrication of crystalline silicon nanowires coated with graphene from graphene oxide on amorphous silicon substrate using excimer laser

Christen Aziz [b], Muhammad A. Othman [a], Aya Amer [a], AbdelRahman M. Ghanim [a,c], Mohamed A. Swillam [a,*]

[a] Department of Physics, American University in Cairo, AUC Avenue, New Cairo, 11835, Cairo, Egypt
[b] Solid State Physics Department, National Research Centre, Giza, Egypt
[c] Department of Physics, Faculty of Science, Ain Shams University, 11566, Cairo, Egypt

A B S T R A C T

In this work, we report a single-step graphene-coated crystalline silicon nanowires (SiNWs) manufacturing technique. We report a one-step fabrication technique of SiNWscoated reduced graphene oxide using a krypton fluoride (KrF) excimer laser. The SiNWs have been manufactured by redistributing the silicon mass within the sample without etching any of the deposited amorphous silicon (a-Si) and then adding a synthesized graphene oxide suspension using the modified Hummers' method. The process is optimized to ensure that the graphene is completely reduced and that the crystalline nanowires are formed. In order to allow full control of the dimension of the generated nanowires, the properties of the excimer laser have been investigated. Additionally, graphene-coated Si nanowires have also been synthesized to be used for gas-sensing applications in the future. In this work, we are eviting the repetition of the previously published work by the same research group for the sake of brevity. But the reader can refer to the previously published work on the study of the effect of different parameters on the SiNWs growth like the study of the effect of changing the normalized frequency on the size of the grown SiNWs in terms of length and diameter as well as other parameters mentioned in the previously published work in the references.

1. Introduction

One-dimensional SiNWs arrangement made it feasible to realize an exciting design that can be used in low-cost applications [1]. Several techniques have been proposed for the fabrication of crystalline SiNWs with minimal reflection. Among these techniques are using wet materials, vapor liquid solid (VLS) development, lithography as well as dry etching. SiNWs were previously produced using lithography and reactive ion etching. Even if controllable NWs have been recorded with improved absorption, these procedures are costly and entail many manufacturing steps [1,2].

The incorporation of nanostructured carbon materials in the fabrication process is another successful technique. Examples include the direct mixture of Si nanowires with graphene Si nanowires, Si chemical vapor concentrations on the carbon sheet, and Si nanowires calcination of high carbon polymers [2–4]./Because of their unique sensing efficiency, graphene-based gas or vapor sensors have attracted attention recently due to their numerous optical and electrical properties, like working in room temperature conditions, and enormous application probabilities. It has different sensing applications for numerous gases (e.g. CO, NH_3, H_2, NO_2, SO_2 as well as vapor of volatile organic compounds) [5]. Although there has been certain advancement in recent years concerning graphene fabrication, some problems still await less advanced applicative technologies due to the operation wavelengths [1–3,6], when compared to

* Corresponding author.
E-mail address: m.swillam@aucegypt.edu (M.A. Swillam).

https://doi.org/10.1016/j.heliyon.2024.e34023
Received 17 June 2024; Accepted 2 July 2024
Available online 4 July 2024

their near-IR equivalents. In addition, conventional silicon-driven systems, which were the main stimulator of the development in this area, multi-material integration continues to play an important role in addressing these challenges [7–18].

Reduced graphene oxide (RGO) plays a major role in preventing the top tips of vertical SiNWs from stacking, thus making SiNWs stand separately under the graphene layer on silicon wafers [19]. Different methods for obtaining reduced graphene have been developed, including the "scotch tape process," which involves simple mechanical cleaving, reduction of graphene oxide (GO), epitaxial growth, and high-temperature vacuum annealing of the Silicon Carbide method [20]. Graphene has several excellent electrical properties as well as high optical transmittance, broad thermal stability, and outstanding mechanical properties [21]. Graphene may create good connections to the substrate of the Schottky photodiode. However, IR-based Graphene/Si Schottky photodetectors have rarely been published [22].

Graphene serves as a passive barrier against oxidizing metal surfaces. One or a few layers of graphene sheets with a broad optical tolerance at visible wavelengths may not impact major substrate light absorption [23–25]. Graphene synthesis implies any method to remove or produce graphene, depending on the specific output's desired purity, size, and fluorescence. Many methods for the development of reduced graphene thin films had been established earlier. Carbon precipitated on the transition metal surfaces in the 1970s in the form of thin graphene sheets [26,27].

Zhipeng Huang et al., 2013 studied the process of spin-coating SiNW arrays with reduced graphene oxide (RGO) on the top of silicon nanowires. The recombination and trapping of photo-generated carriers at the surface of SiNWs were reduced after the coating of RGO. The results of measurements of electrochemical impedance spectroscopy indicated that a reduction of trapping and recombination of photo-generated carriers as well as notable enhancement of photo-electrochemical properties assigned to low load transfer resistance at the SiNWs at RGO interface and RGO−electrolyte interface has been achieved [28].

Jungkil Kim et al., in 2014 successfully synthesized a wafer-scale graphene on SiNWs heterostructure for molecular sensing. The sensor responses are clarified based on the doping mechanism for surface transfer. These findings strongly suggest that heterostructures of graphene/Si NW can be implemented over extended scales as different types of SiNW-based devices such as molecular, photonic, and medical sensors [19]. For vertical SiNWs to be used in practical devices such as sensors, a continuous electrode must be formed on the ends of the SiNWs to provide consistent electrical contact between the electrode and the SiNWs. In earlier research, the tips of NWs were coated with polymer (or other insulators), then partially opened by O_2 plasma or other etching techniques, and then the metal layer was placed on the partially opened tips of NWs [19].

The electrical properties of the contact between undefined graphene, irregular-shaped and randomly arranged SiNWs with very sharp edges were investigated by Jungkil Kim et al. [19]. The investigation demonstrated that the electrode made non-uniform contact with the NWs, leading to low-quality device performances [19]. In the last decade, the photo-reduction of graphene oxide to synthesize reduced graphene oxide has appeared as an appealing alternative method because photo-reduction does not count on toxic chemicals, high power sources, or high temperatures [29–34]. Photo-reduction of graphene oxide can generate patterned graphene structures utilizing directed laser beams [29,34–38]. The benefits of this technique are that it is accurate, flexible, and cost-effective and requires no predefined patterned masks to be used for rapid prototyping. Graphene serves a vital structural role in preventing vertical SiNW tips from becoming bundled, allowing SiNWs to stand on Si wafers independently from one other under graphene, a critical structural characteristic for the consistent Schottky-type connection between SiNWs and graphene [19,39].

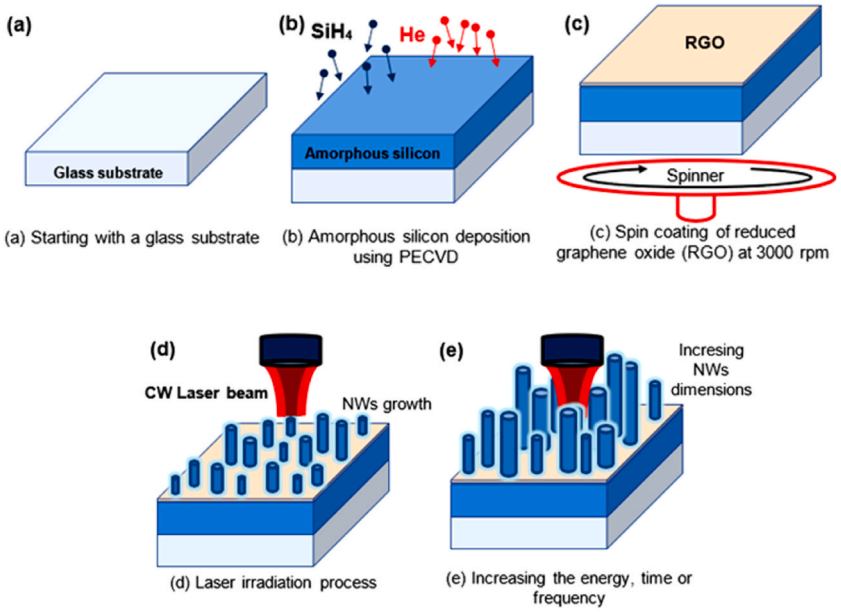

Fig. 1. Sketch of the fabrication process of SiNWs. Amorphous silicon-coated RGO was first deposited using PECVD on glass substrates, SiNWs at RGO are formed after laser irradiation.

In this paper, we are reporting a one-step fabrication process of SiNWs using direct exposure of amorphous silicon with a graphene oxide layer deposited chemically on the surface of the amorphous silicon. The laser irradiation is done using a continuous wave (CW) excimer laser on the amorphous silicon surface resulting in crystalline SiNWs on the silicon dioxide substrates. The intended application is for gas sensing. When subjected to laser beams, silicon molds and solidifies into nanowires and reduces graphene oxide to graphene depending on the laser intensity, wavelength, and exposure period.

2. Fabrication and results

2.1. Fabrication of silicon NWs

The main objective of the work is to fabricate the proposed structure with a single fabrication phase to highlight its edge when compared to the more sophisticated fabrication techniques. Starting with a glass substrate, a thin layer of amorphous silicon is deposited over the glass substrate using plasma-enhanced chemical vapor deposition (PECVD) using SiH_4 and He gases. The thickness of this thin layer of amorphous silicon is 1 μm. Then, the sample is mounted on a motorized computer-controlled spinner and irradiated with multiple pulses using a KrF Excimer laser for nanowire formation. Then, a thin film of RGO is spin-coated on the substrate at 3000 rpm. Afterward, the coated substrate is subjected to KrF laser excimer for fabrication of the nanowires and reduction of the graphene oxide to graphene. Multiple fabrication trials were made until the optimum values were reached at pulse frequency (f = 30 Hz) exposure time (T = 40 s) and the laser energy density (E = 85 mJ) as shown in Fig. 1.

2.1.1. Samples characterization using scanning electron microscopy (SEM)

The morphology was characterized using a Zeiss Leo field emission scanning electron microscopy (FESEM). Au sputtering for 30 s was performed prior to SEM imaging to make the surface conductive.

All images shown in this work are cross-sections and were taken with a 20° tilt. The optical properties were measured using a PerkinElmer Lambda 950 (UV–vis−near-IR) spectrophotometer. A ProRaman-L analyzer was used for the Raman measurements. Multiple fabrication trials were made until the optimum values were reached at pulse frequency (f = 30 Hz) exposure time (T = 40 s) and the laser energy density (E = 75 mJ). The produced nanowires are shown and graph-coated and uncoated nanowires are differentiated by their transmission graphs. Fig. 2 shows the SEM of the fabricated nanowires at (T = 30 s, f = 40 Hz, E = 75 mJ). SiNWs coated and uncoated RGO was obtained with an average length (~3 μm) almost equal to the average diameter.

Fig. 3(a) shows the SEM of the obtained SiNWs coated RGO at 50 mJ cm^{-2} energy density, frequency 40 Hz, and exposure time 30 s while Fig. 3(b) shows the SEM of the obtained SiNWs coated RGO at 80 mJ cm^{-2} energy density, frequency 40 Hz, and exposure time 30s. As noticed that when energy density increases from 50 mJ cm^{-2} to 75 mJ cm^{-2} a further increase in both the diameter and the

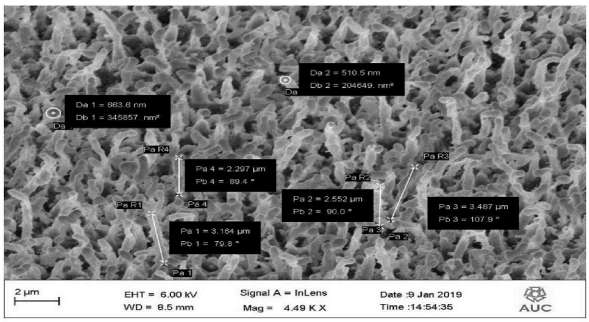

(a)

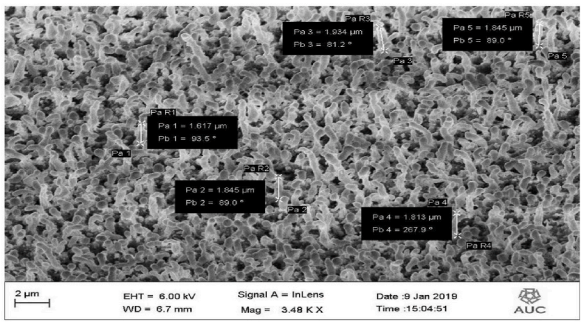

(b)

Fig. 2. SEM images (tilt angle = 20°) of NWs fabricated at E = 75 mJ, T = 30s, f = 40 Hz (a) With graphene and (b) Without Graphene.

length occurs. Any further increase in the energy density caused the SiNWs coated RGO to have irregular shapes because the deposited nanomaterial was already consumed and the added energy density caused the remaining material to redeposit on the base of the wires only forming these irregular NWs as shown in Fig. 3(b) for energy density 80 mJ cm^{-2}. We concluded that increasing the frequency has a significant effect on increasing the length of the Si-coated NWs. It is obvious that as the frequency increases, the length of the NW increases, and the diameter almost remains unchanged as shown in Fig. 3 [1].

2.2. The scattering of the fabricated vertical coated SiNWs

The optical properties of the fabricated NWs have been analyzed. Measurements of scattering spectrums of RGO-coated and uncoated Si nanowires were obtained. A super-continuum NKT laser source (1.0 μm–5.0 μm) was directed to the coated and uncoated nanowires and the scattering spectrum was measured using a Thorlabs optical spectrum analyzer (OSA). As shown in Fig. 4. RGO-coated NWs have a maximum scattering intensity in the MIR. In the modeling and physical verification section, a comprehensive explanation of the obtained results will be provided in detail.

2.3. Raman spectroscopy analysis

Fig. 5 illustrates the SiNWs Raman peak at 521 cm^{-1}. In addition, porous SiNWs have many other Raman peaks; the main peak at 522 cm^{-1} corresponds to the first-order transverse optical mode (1TO) moving down to a lower frequency than the C–Si. The second-order transverse acoustic mode (2 TA) corresponds to another broadband peak at 296 cm^{-1} and the last broad band at 940 cm-1 can be attributed to the second-order transverse optical phonon mode (2TO) [6]. Also shows the Raman spectroscopy measurements of the nanowires with the peak of silicon and two peaks of RGO at 520 nm, 1360 nm, and 1608 nm respectively. The intensity ratio of I_{2D}:$I_G \approx 2$, along with the weak D-band scattering at ~1344 cm^{-1}, indicates the high crystal quality of the thin film [24]. The characteristic

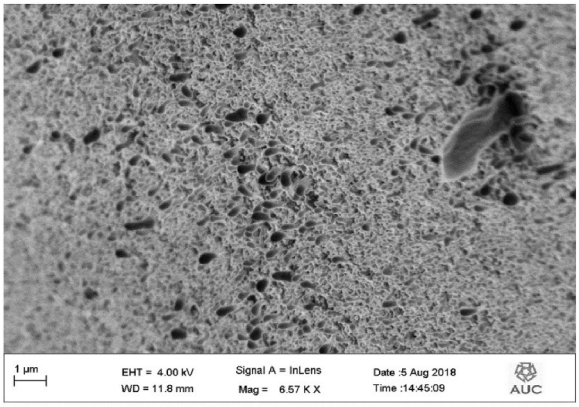

(a)

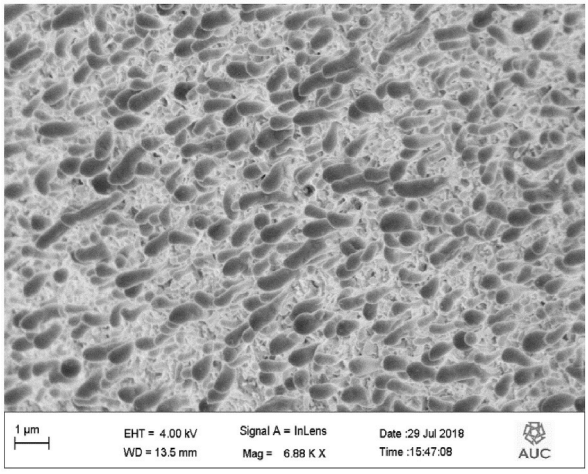

(b)

Fig. 3. SEM of SiNWs (tilt angle = 20°) coated RGO using (a) 50 mJ.cm-2, 40 Hz, 30 s (b) 80 mJ.cm-2, 40 Hz, 30 s.

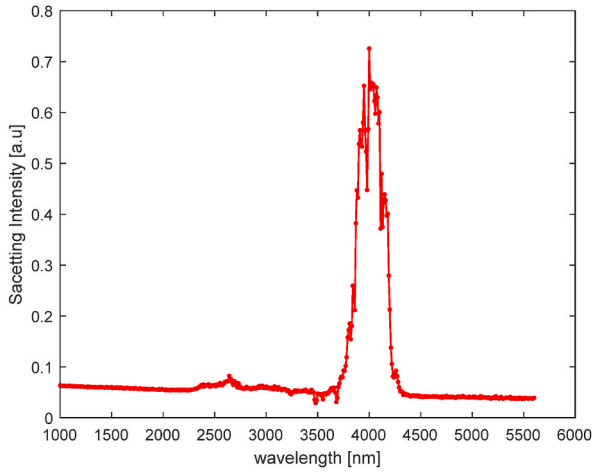

Fig. 4. Scattering spectrum RGO coated SiNWs at $E = 75$ mJ, $T = 30$ s, $f = 30$ Hz.

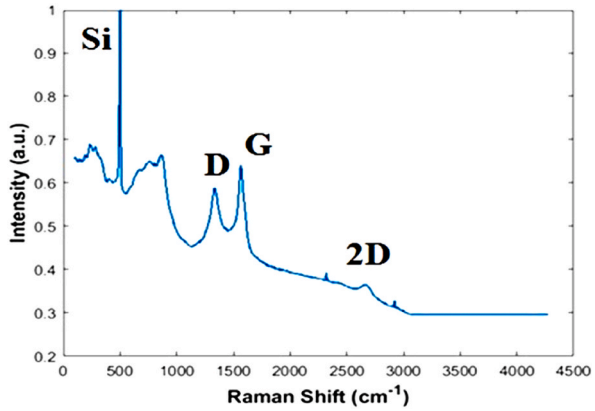

Fig. 5. Raman spectrum of graphene-coated SiNWs at $E = 75$ mJ, $T = 30$ s, $f = 30$ Hz.

peaks at 1360, and 1608 cm^{-1}, corresponding to the D, and G bands of the RGO lattice, respectively, were observed in all irradiated samples, indicating a direct reduction of the GO into RGO.

2.4. Atomic force microscopy (AFM)

For mechanical characterization of SiNWs using AFM nano-indentation, where commercially available AFM (Innova, Santa Barbara, CA, USA) with Nano-drive controller (Veeco, Santa Barbara, CA, USA) and closed-loop scanner used in this work. For both imaging and indentation, we have used Al-coated silicon cantilevers (TESPA, Veeco, Santa Barbara, CA, USA) with a nominal tip radius of ≈10 nm with a scanning rate = 1.001 Hz and scan size in the range of 20 μm × 20 μm to 500 nm × 500 nm.AFM was used to distinguish the surface topography and the roughness constants of the synthesized SiNWs. Vs. SiNWs @RGO.In AFM, a small probe is scanned across the sample, and the surface information of the sample is congregated from the interaction of the probe with the sample surface. The results obtained are in the form of physical topography and measurements of Ra & Rq of the sample. The surface is defined by parameters dependent on the vertical deviations from the mean line of the roughness profile. Many of the parameters used in statistics for characterizing population samples are closely related. Ra: the average numerical value of the filtered roughness profile calculated from the center line deviations within the duration of the assessment, And Rq is the root mean squared.

Fig. 6 shows the AFM images of SiNWs synthesized using the KrF laser method, $R_a = 481.79$ nm & $R_q = 381.25$ nm. The surface is defined by parameters dependent on the vertical deviations from the mean line of the roughness profile. Meanwhile, in the roughness analysis, any of the parameters used in statistical methodology for characterizing the population samples are closely related where R_a is the average numerical value of the filtered roughness profile and R_q is root mean squared as shown in Fig. 6(b). On the other hand, Fig. 7 shows the AFM images of graphene oxide-coated SiNWs where the roughness analysis shows $R_a = 361.05$ nm & $R_q = 433.7$ nm.

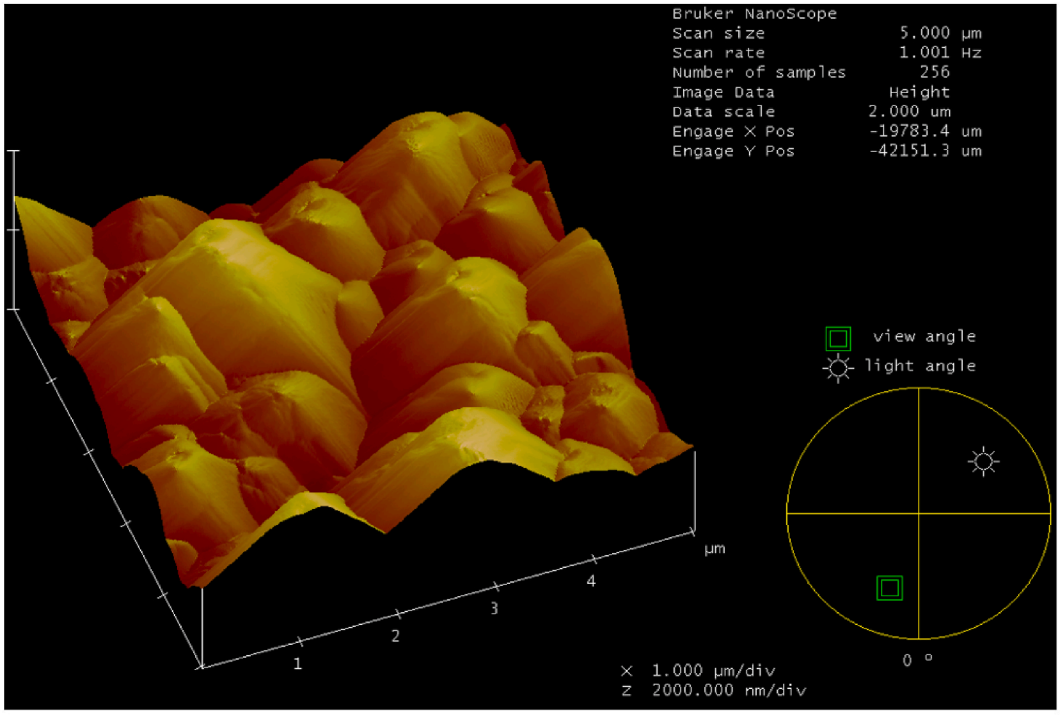

(a)

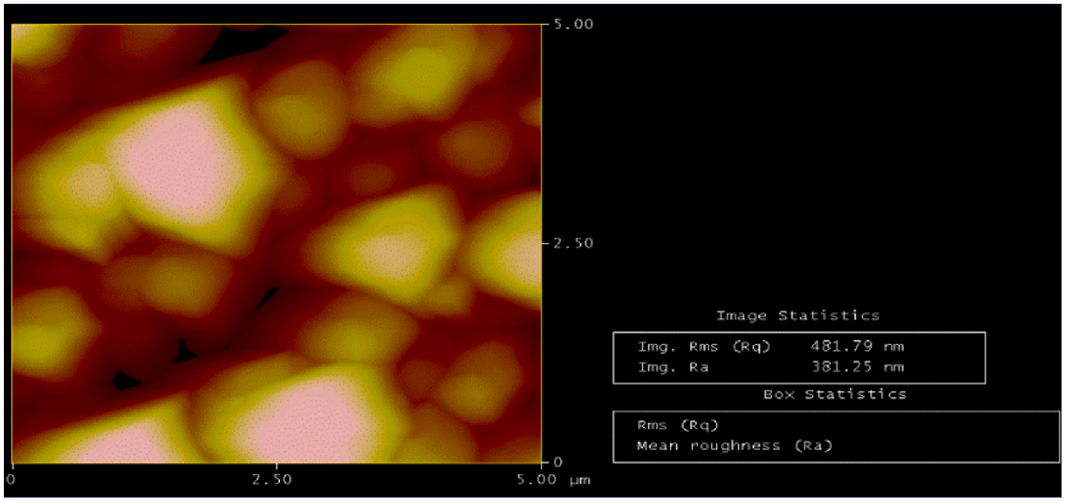

(b)

Fig. 6. (a) Three-dimensional AFM image of non-coated SiNWs synthesized using KrF laser irradiation method where scan rate is 1.001 Hz and scan size 5 µm (b) Roughness analysis results where $R_a = 481.79$ nm and $R_q = 381.25$ nm.

2.5. X-ray diffraction analysis (XRD)

Fig. 8 shows the X-ray diffraction (XRD) analysis (Count vs 2 theta) that helps in understanding the nature of the modification that happened on the amorphous silicon and its transformation to crystalline nature. Fig. 8(a) shows the uncoated SiNWs with RGO where broader response. No significant peaks have been noticed in the case of the generated SiNWs without reduced graphene oxide. That means the structure tends to have an amorphous nature. In Fig. 8(b) significant peaks appear at different 2 theta scales meaning that the structure tends to be polycrystalline in shape.

The synthesized SiNWs have diffraction peaks observed at approximately 33° which could be related to the crystalline silicon (100) as the main wafer, and another peak at 49° & 58° related to (220) (311) respectively. And a peak appears at 29° for RGO (002).

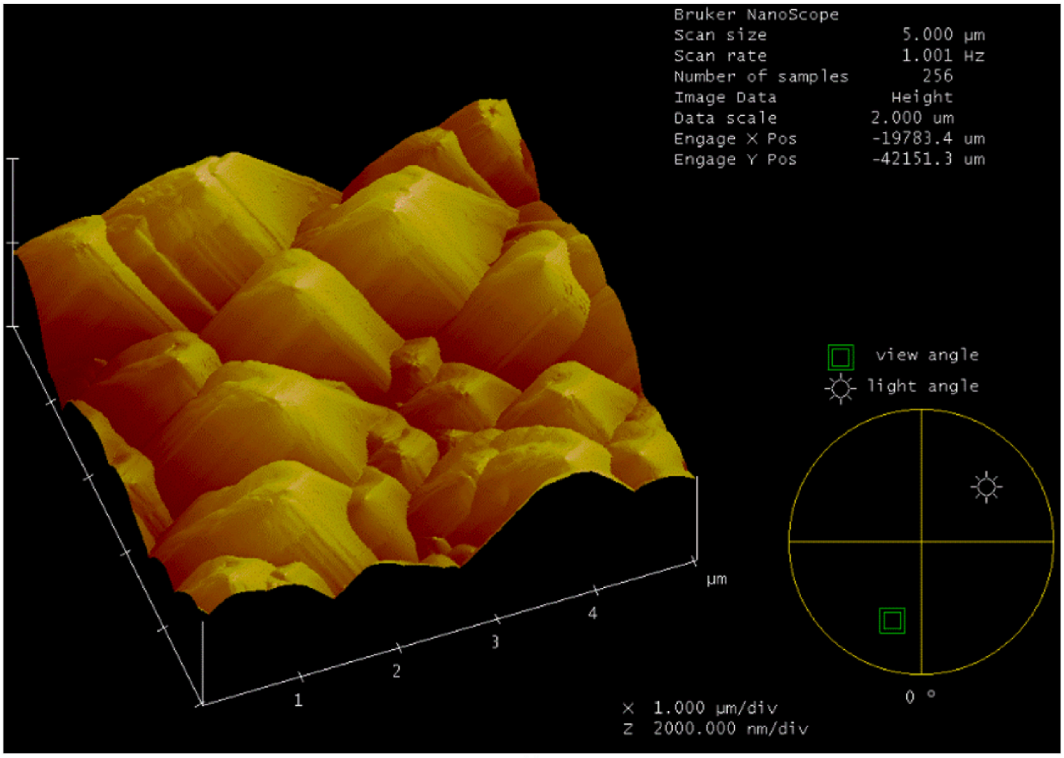

(a)

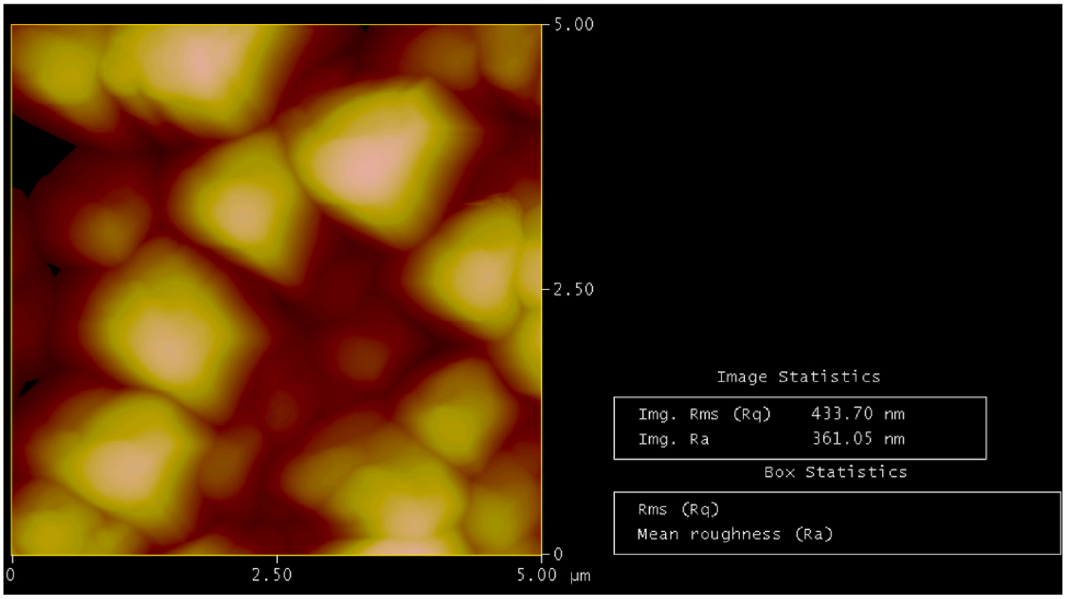

(b)

Fig. 7. (a) Three-dimensional AFM image of graphene oxide coated SiNWs synthesized using KrF laser irradiation method where scan rate is 1.001 Hz and scan size 5 µm (b) Roughness analysis results where $R_a = 361.05$ nm and $R_q = 433.7$ nm.

3. Modeling and physical verification

In order to investigate the optical characteristics and near-field computations of the coated SiNWs, we performed three-dimensional finite-difference time-domain simulations using commercially accessible software based on Maxwell's equations (Lumerical FDTD Solutions) [40]. we first study the optical characteristics of SiNWs with plane wave source polarised along the *z*-direction as seen in Fig. 9. The range of wavelengths covered by the incident radiation spectrum ranged from 3 µm to 6 µm. To

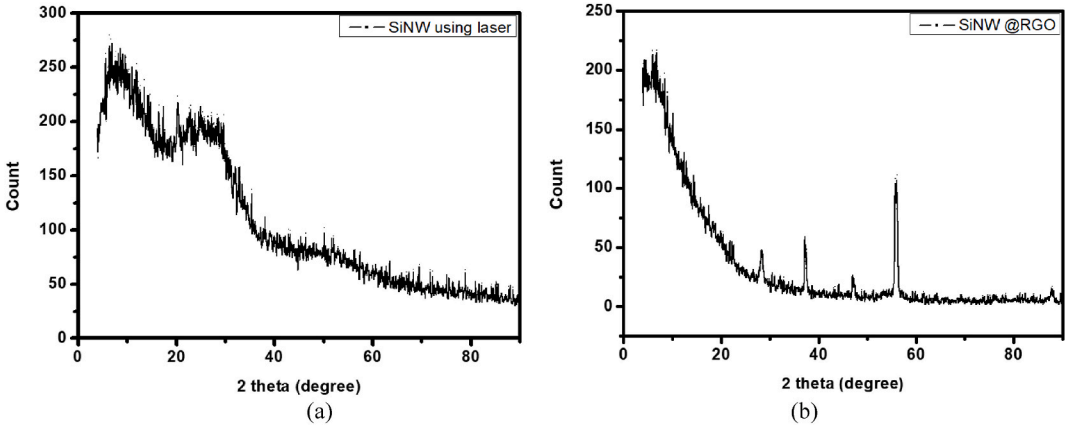

Fig. 8. X-ray diffraction analysis for (a) SiNW using laser and (b) SiNW with reduced graphene oxide showing a more crystalline nature.

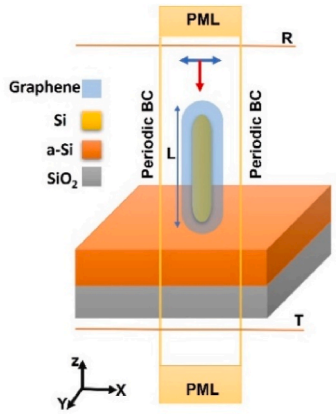

Fig. 9. The schematic diagram illustrates the setup of the FDTD Lumerical simulation for RGO-coated silicon nanowires.

minimize computation time, the 3D simulation box was bounded by anti-symmetric, symmetric, and perfectly matched boundary conditions (BCs) in the x, y, and z directions, respectively. Additionally, we employed mesh override sections to achieve a high level of resolution in specific areas of the structure, a mesh size of 10 nm was used around the SiNW. To estimate the transmittance (T) and reflectance (R) spectra, two FDTD power monitors are utilized as shown in Fig. 9.

This paper introduces coated SiNWs, which are placed on a SiO_2 substrate. The geometrical design parameters used for simulation are as follows: The dimensions of the substrate are 0.6 μm × 0.6 μm × 1 μm in the x, y, and z directions, respectively, and it is modeled using Palik [41]. A layer of amorphous silicon was added on top of the substrate, with dimensions of 0.6 μm × 0.6 μm × 1 μm in the x, y, and z directions, respectively. The silicon nanowire is 1.2 μm long (L) and has a radius of 0.25 μm coated with an RGO layer. In this simulation, we studied how power is scattered in a silicon nanowire as indicated in Fig. 10. Initially, the intensity of the scattered light was measured in decibels. and it is converted to a linear scale. The measurement of reflected light in a spectrum analyzer involves the calculation of the difference between the light scattered by the fabricated coated SiNWs (R(C-SiNWs)) and the light scattered by the substrate (R(subs)) as:

$$\text{Scattered intensity} = \frac{R(\text{C}-\text{SiNWs}) - R(\text{subs})}{R(\text{subs})} \tag{1}$$

Once the normalization process is completed and the obtained intensity is appropriately fitted, the measured scattered intensity of the RGO-coated SiNWs can be shown in Fig. 10(a).

SiNWs have an anticipated property since they have low transmitted power and high reflected power at a wavelength of 4.5 μm as shown in Fig. 10(b). This particular behavior is prompted by the nanowires' waveguiding capabilities, which allow for effective light reflection. Light is mainly reflected when it interacts with SiNWs rather than transmitted through the structure. This high scattered power might be useful in applications in which maximum scattering is desired, such as chemical sensing, spectroscopy, and thermal imaging.In Fig. 11, the electric and magnetic field profiles are depicted for SiNW with a diameter of 0.5 μm. Particularly, at the resonant wavelength ($\lambda = 4.5$ μm), the high reflected power is attributed to the electric and magnetic dipole resonance. SiNWs show unique features associated with electric and magnetic dipoles [42]. The electric dipole moment is generated when positive and

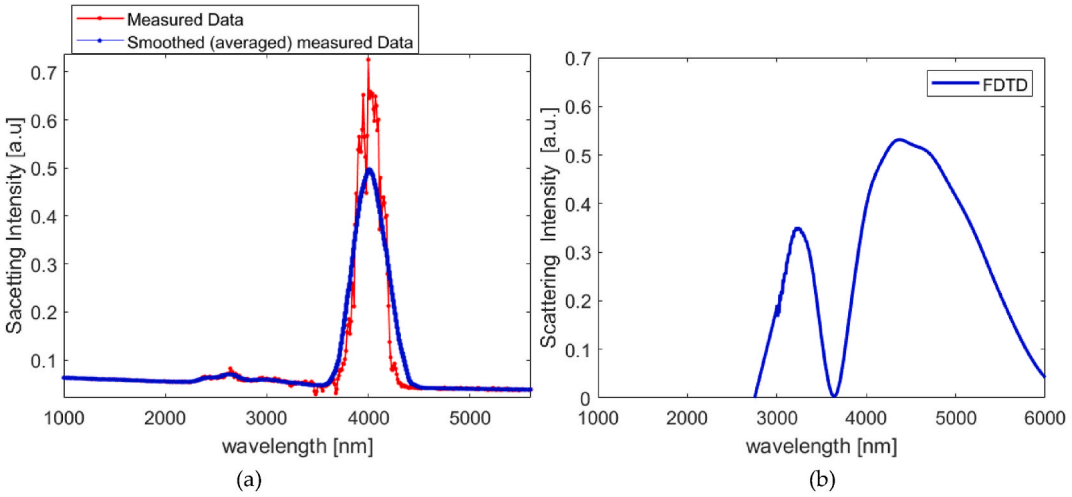

Fig. 10. (a) The measured scattering spectrum as a function of wavelength and (b) the FDTD simulation of the scattering spectrum for the RGO-coated SiNWs.

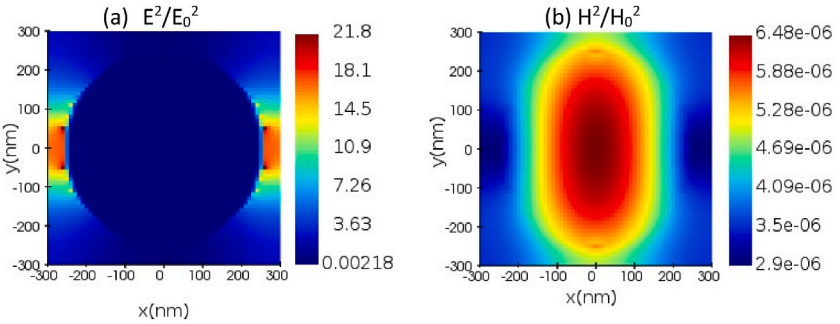

Fig. 11. The distribution of (a) the local electric field and (b) the magnetic field in the XY-plane induced by normal incidence at $\lambda = 4.5$ μm.

negative charges within the nanowire are displaced, leading to the formation of an oscillating electric field. The interaction between this dipole moment and external electromagnetic fields can result in light emission, absorption, and scattering. On the other hand, the magnetic dipole moment observed in SiNWs is generated by the incident electromagnetic field-induced circulating currents. The magnetic field produced by these circulating currents interacts with the incident field to affect the nanowire's overall magnetic response [43,44].

4. Conclusion

In this work, SiNWs coated RGO with improved optical absorption in MIR due to the presence of RGO coating were reported using a one-step manufacturing phase. The fabrication method is simple, cost-effective, and does not involve specific equipment, without including numerous chemicals, masks, vacuum-controlled enclosures, or any catalysts. The key objective of this study is the characterization of the SiNWs coated using graphene oxide thin film to be used in sensing applications. Thus, the proposed laser-reduced graphene films can be utilized as an optical sensing device on wearable electronic devices, solar cells, LEDs, gas sensors, and implantable biomedical devices. It could open the way for further extensive research in functionalized 2D materials. This work can be extended to analyze the effects of background gases on the laser RGO fabricated nanowires absorption in the MIR. Meanwhile, it can be used in gas-sensing applications.

Data availability

The datasets used and/or analyzed during the current study available from the corresponding author on reasonable request.

CRediT authorship contribution statement

Christen Aziz: Data curation, Investigation, Methodology, Visualization, Writing – original draft, Writing – review & editing.

Muhammad A. Othman: Investigation, Methodology, Writing – original draft, Writing – review & editing. **Aya Amer:** Investigation, Methodology, Writing – original draft, Writing – review & editing. **AbdelRahman M. Ghanim:** Data curation, Methodology, Software, Validation, Visualization, Writing – original draft, Writing – review & editing. **Mohamed A. Swillam:** Conceptualization, Data curation, Formal analysis, Funding acquisition, Investigation, Methodology, Project administration, Resources, Software, Supervision, Validation, Visualization, Writing – original draft, Writing – review & editing.

Declaration of competing interest

The authors declare that they have no known competing financial interests or personal relationships that could have appeared to influence the work reported in this paper.

Acknowledgments

We thank Mr. Raghi Samir for his contribution during the measurements of the fabricated SiNWs.

References

[1] S. Magdi, J. El-Rifai, M.A. Swillam, Lithography-free fabrication of crystalline silicon nanowires using amorphous silicon substrate for wide-angle energy absorption applications, ACS Appl. Nano Mater. 1 (6) (2018) 2990–2996.
[2] S.A. Razek, M.A. Swillam, N.K. Allam, Vertically aligned crystalline silicon nanowires with controlled diameters for energy conversion applications: experimental and theoretical insights, J. Appl. Phys. 115 (19) (2014).
[3] X. Xin, X. Zhou, F. Wang, X. Yao, X. Xu, Y. Zhu, Z. Liu, A 3D porous architecture of Si/graphene nanocomposite as high-performance anode materials for Li-ion batteries, J. Mater. Chem. 22 (16) (2012) 7724–7730.
[4] Y. Zhu, W. Liu, X. Zhang, J. He, J. Chen, Y. Wang, T. Cao, Directing silicon–graphene self-assembly as a core/shell anode for high-performance lithium-ion batteries, Langmuir 29 (2) (2013) 744–749.
[5] W. Wang, P.N. Kumta, Nanostructured hybrid silicon/carbon nanotube heterostructures: reversible high-capacity lithium-ion anodes, ACS Nano 4 (4) (2010) 2233–2241.
[6] A.M. Gouda, N.K. Allam, M.A. Swillam, Efficient fabrication methodology of wide-angle black silicon for energy harvesting applications, RSC Adv. 7 (43) (2017) 26974–26982.
[7] T. Wang, D. Huang, Z. Yang, S. Xu, G. He, X. Li, L. Zhang, A review on graphene-based gas/vapor sensors with unique properties and potential applications, Nano-Micro Lett. 8 (2016) 95–119.
[8] R. Gamal, S. Shafaay, Y. Ismail, M.A. Swillam, Silicon plasmonics at mid infrared using silicon-insulator-silicon platform, J. Nanophotonics 11 (1) (2017) 016006.
[9] S.M. Sherif, M.A. Swillam, Metal-less silicon plasmonic mid-infrared gas sensor, J. Nanophotonics 10 (2) (2016) 26025.
[10] M.A. Ayad, M.A. Swillam, Mid-infrared plasmonic power splitters, IEEE Photonics Technol. Lett. 28 (21) (2016) 2431–2434.
[11] M.A. Swillam, Mid infrared applications of silicon thermoplasmonics, in: Proceedings of the 2016 IEEE Photon. North (PN), Canada, 2016.
[12] H. Lin, Z. Luo, T. Gu, L.C. Kimerling, K. Wada, A. Agarwal, J. Hu, Mid-infrared integrated photonics on silicon: a perspective, Nanophotonics 7 (2) (2017) 393–420.
[13] S. Magdi, F. El-Diwany, A. Swillam, M. Broadband MIR harvester using silicon nanostructures, Sci. Rep. 9 (1) (2019) 5829.
[14] R.S. El Shamy, D. Khalil, M.A. Swillam, Mid infrared optical gas sensor using plasmonic Mach-Zehnder interferometer, Sci. Rep. 10 (2020) 1293.
[15] R. Gamal, Y. Ismail, M.A. Swillam, Silicon waveguides at the mid-infrared, J. Lightwave Technol. 33 (15) (2015) 3207–3214.
[16] S. Shafaay, M. Swillam, Gas sensing devices using doped silicon material at mid-infrared region, Proceedings of the SPIE Silicon Photon 10923 (2019) 194–202.
[17] R. Gamal, Y. Ismail, M.A. Swillam, Silicon waveguides at the mid-infrared, J. Lightwave Technol. 33 (15) (2015) 3207–3214.
[18] A.B. Ayoub, M.A. Swillam, Silicon plasmonics on-chip mid-IR gas sensor, IEEE Photonics Technol. Lett. 30 (10) (2018) 931–934.
[19] J. Kim, S.D. Oh, J.H. Kim, D.H. Shin, S. Kim, S.H. Choi, Graphene/Si-nanowire heterostructure molecular sensors, Sci. Rep. 4 (1) (2014) 5384.
[20] G. Ko, H.Y. Kim, J. Ahn, Y.M. Park, K.Y. Lee, J. Kim, Graphene-based nitrogen dioxide gas sensors, Curr. Appl. Phys. 10 (4) (2010) 1002–1004.
[21] C. Tharwat, M.A. Swillam, Y. Badr, S.M. Ahmed, I.K. Bishay, F.A. Sadallah, E.A. Elsaid, Novel optical technique for 2D graphene reduction, Proceedings of the SPIE Opt. Components and Mater 10100 (2017) 174–178.
[22] P. Lv, X. Zhang, X. Zhang, W. Deng, J. Jie, High-sensitivity and fast-response graphene/crystalline silicon Schottky junction-based near-IR photodetectors, IEEE Electron. Device Lett. 34 (10) (2013) 1337–1339.
[23] X. Zhong, G. Wang, B. Papandrea, M. Li, Y. Xu, Y. Chen, X. Duan, Reduced graphene oxide/silicon nanowire heterostructures with enhanced photoactivity and superior photoelectrochemical stability, Nano Res. 8 (2015) 2850–2858.
[24] M. Desouky, M.R. Anisur, M. Alba, R.S. Raman, M.A. Swillam, N.H. Voelcker, A. Kasry, Near-field mapping of localized plasmon resonances in metal-free, nanomembrane graphene for mid-infrared sensing applications, ACS Appl. Nano Mater. 1 (11) (2018) 6454–6462.
[25] Desouky, M.; Swillam, M. A.; Kasry, A. Tunable mid IR absorption in single-layer, nanomeshed graphene. In Proceedings of the J. Of Phy.: Conference Series IOP Publishing. vol. 1253, 012023.
[26] M. Eizenberg, J.M. Blakely, Carbon monolayer phase condensation on Ni (111), Surf. Sci. 82 (1) (1979) 228–236.
[27] M. Eizenberg, J.M. Blakely, Carbon interaction with nickel surfaces: monolayer formation and structural stability, J. Chem. Phys. 71 (8) (1979) 3467–3477.
[28] Z. Huang, P. Zhong, C. Wang, X. Zhang, C. Zhang, Silicon nanowires/reduced graphene oxide composites for enhanced photoelectrochemical properties, ACS app. Mater. Interfac. 5 (6) (2013) 1961–1966.
[29] Y.L. Zhang, L. Guo, H. Xia, Q.D. Chen, J. Feng, H.B. Sun, Photoreduction of graphene oxides: methods, properties, and applications, Adv. Opt. Mater. 2 (1) (2014) 10–28.
[30] M.Y. Elsayed, A.M. Gouda, Y. Ismail, M.A. Swillam, Silicon-based SERS substrates fabricated by Electroless etching, J. Lightwave Technol. 35 (14) (2017) 3075–3081.
[31] R.S. El Shamy, D. Khalil, M.A. Swillam, Mid infrared optical gas sensor using plasmonic Mach-Zehnder interferometer, Sci. Rep. 10 (1) (2020) 1293.
[32] E. Kymakis, K. Savva, M.M. Stylianakis, C. Fotakis, E. Stratakis, Flexible organic photovoltaic cells with in situ nonthermal photoreduction of spin-coated graphene oxide electrodes, Adv. Funct. Mater. 23 (21) (2013) 2742–2749.
[33] X. Li, H. Ren, X. Chen, J. Liu, Q. Li, C. Li, M. Gu, Athermally photoreduced graphene oxides for three-dimensional holographic images, Nat. Commun. 6 (1) (2015) 6984.
[34] H. Zhang, Y. Miyamoto, Graphene production by laser shot on graphene oxide:an ab initio prediction", Phys. Rev. B 85 (3) (2012) 033402.
[35] D.A. Sokolov, K.R. Shepperd, T.M. Orlando, Formation of graphene features from direct laser-induced reduction of graphite oxide, J. Phys. Chem. Lett. 1 (18) (2010) 2633–2636.
[36] W. Neelam Gao, N. Singh, L.Z. Liu, A.L.M. Reddy, L. Ci, R. Vajtai, Q. Zhang, B. Wei, P.M. Ajayan, Direct laser writing of microsupercapacitors on hydrated graphite oxide films", Nat. Nanotechnol. 6 (8) (2011) 496–500.

[37] B.Y. Zhou, Q. Bao, B. Varghese, L.A.L. Tang, K. Chow Tan, C.H. Sow, K.P. Loh, Microstructuring of graphene oxide nanosheets using direct laser writing", Adv. Mater. 22 (1) (2010) 67–71.
[38] Y. Zhang, L. Guo, S. Wei, Y. He, H. Xia, Q. Chen, F.S. Xiao, Direct imprinting of microcircuits on graphene oxides film by femtosecond laser reduction, Nano Today 5 (1) (2010) 15–20.
[39] S. Magdi, J. El-Rifai, M.A. Swillam, One step fabrication of Silicon nanocones with wide-angle enhanced light absorption, Sci. Rep. 8 (1) (2018) 4001.
[40] Lumerical Solutions I, https://www.lumerical.com.
[41] E.D. Palik, Handbook of Optical Constants of Solids, Academ. Press, 1998.
[42] J. Li, N. Verellen, P. Van Dorpe, Enhancing magnetic dipole emission by a nano-doughnut-shaped silicon disk, ACS Photonics 4 (8) (2017) 1893–1898.
[43] A.E. Alsayed, A.M. Ghanim, A. Yahia, M.A. Swillam, Giant localized electromagnetic field of highly doped silicon plasmonic nanoantennas, Sci. Rep. 13 (1) (2023) 5793.
[44] R.S. El Shamy, M.A. Swillam, D.A. Khalil, Mid infrared integrated MZI gas sensor using suspended silicon waveguide, J. Lightwave Technol. 37 (17) (2019) 4394–4400.